One Earth

Article

Historical and future global burned area with changing climate and human demography

Graphical abstract

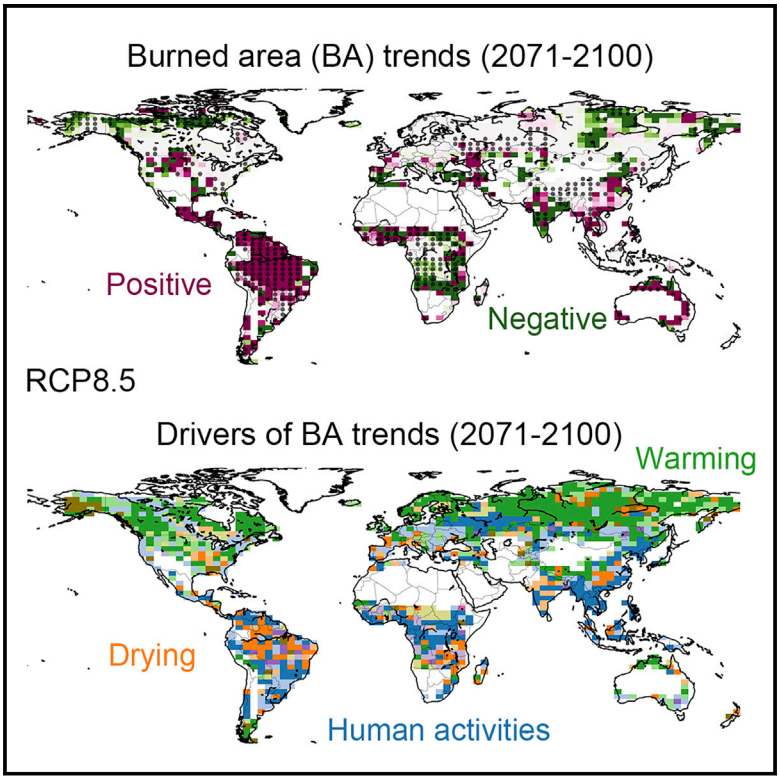

Highlights

- We evaluate historical and future burned area (BA) trends and their drivers
- Recent BA has decreased in central South America and mesic African savannas
- High-latitude warming, (sub)tropical drying, and human ignitions will increase future BA
- Fire suppression near human settlements can offset large potential BA increases

Authors

Chao Wu, Sergey Venevsky, Stephen Sitch, Lina M. Mercado, Chris Huntingford, A. Carla Staver

Correspondence

chaowu.thu@gmail.com (C.W.), venevsky@tsinghua.edu.cn (S.V.)

In brief

Understanding the drivers of the spatial distribution and temporal trends in wildfire activity is necessary to enable robust predictions of future fire activity in the Earth system. Using a climate-fire-carbon cycle-coupled model, Wu et al. show that accelerated high-latitude warming and tropical and subtropical drying and human ignitions will increase the future global burned area, while fire suppression in the vicinity of human settlements is important in offsetting the potential for dramatic burned area increases.

Wu et al., 2021, One Earth *4*, 517–530
April 23, 2021
https://doi.org/10.1016/j.oneear.2021.03.002

CellPress

One Earth

Gold Standard for the Global Goals
3 tons of CO_2 offset

CellPress
OPEN ACCESS

Article

Historical and future global burned area with changing climate and human demography

Chao Wu,[1,2,4,5,*] Sergey Venevsky,[1,*] Stephen Sitch,[2] Lina M. Mercado,[2,3] Chris Huntingford,[3] and A. Carla Staver[4]
[1]Ministry of Education Key Laboratory for Earth System Modeling, Department of Earth System Science, Tsinghua University, Beijing 100084, China
[2]College of Life and Environmental Sciences, University of Exeter, Exeter EX4 4QF, UK
[3]UK Centre for Ecology and Hydrology, Wallingford, Oxfordshire OX10 8BB, UK
[4]Department of Ecology and Evolutionary Biology, Yale University, New Haven, CT 06511, USA
[5]Lead contact
*Correspondence: chaowu.thu@gmail.com (C.W.), venevsky@tsinghua.edu.cn (S.V.)
https://doi.org/10.1016/j.oneear.2021.03.002

SCIENCE FOR SOCIETY Wildfire is an important natural disturbance for many ecosystems, helping to shape biome distributions and controlling the carbon balance. Major changes in fire activity could also have a strong impact on human societies. Changes in fire activity are influenced both by climatic changes and by changes in human demography via, e.g., population growth and urbanization. We show that in recent decades, global burned area has actually decreased, especially in central South America and mesic African savannas. However, our future simulations indicate that future climate and demographic change will reverse this trend and that burned area is likely to increase due to accelerated high-latitude warming and tropical and subtropical drying and human ignitions. These projections will inform more detailed, local work to develop wildfire management strategies and to assess ecological responses to global change, and will contribute to the discussion of what constitutes a safe upper limit to global warming.

SUMMARY

Wildfires influence terrestrial carbon cycling and represent a safety risk, and yet a process-based understanding of their frequency and spatial distributions remains elusive. We combine satellite-based observations with an enhanced dynamic global vegetation model to make regionally resolved global assessments of burned area (BA) responses to changing climate, derived from 34 Earth system models and human demographics for 1860–2100. Limited by climate and socioeconomics, recent BA has decreased, especially in central South America and mesic African savannas. However, future simulations predict increasing BA due to changing climate, rapid population density growth, and urbanization. BA increases are especially notable at high latitudes, due to accelerated warming, and over the tropics and subtropics, due to drying and human ignitions. Conversely, rapid urbanization also limits BA via enhanced fire suppression in the immediate vicinity of settlements, offsetting the potential for dramatic future increases, depending on warming extent. Our analysis provides further insight into regional and global BA trends, highlighting the importance of including human demographic change in models for wildfire under changing climate.

INTRODUCTION

Wildfire is a natural and inevitable feature of the environment in many terrestrial ecosystems and has a strong influence on biogeography, ecosystem functioning, and land-atmosphere carbon and energy fluxes.[1,2] However, fire also potentially puts humans at risk from atmospheric pollutants[3] and health and infrastructure hazards.[1,4] Overall, global burned area (BA) has declined significantly (by 24.3% ± 8.8%) over the past 18 years[5] and represents the net of differential regional responses. Indeed, despite overall decreases in fire activity, the incidence of major and catastrophic fire events has increased in many regions, with widespread media attention to fires in the Amazon, western North America, the Mediterranean, and Australia. Unfortunately, future fire trends remain uncertain, both at the regional scale and in terms of their spatial distribution;[6] indices of climatic fire risk and fire activity are confidently predicted to exacerbate in a warmer and often drier world,[7–9] whereas human drivers of BA are instead projected to suppress fires.[5,10] Better projections of future regional BA, incorporating both climate and human effects on fire extent, are urgently required to enable any appropriate adaptation and mitigation planning.

Climate, particularly temperature (T; °C) and precipitation (P; mm), is the central determinant of fire activity through its controls on vegetation productivity (i.e., providing fuel for fires) and fuel moisture (i.e., influencing the probability of the fire occurrence).[11] Vegetation productivity generally increases with rainfall and thereby provides fuel for fires,[12] although the magnitude of this effect changes across gradients of plant productivity.[13] Meanwhile, reduced fuel moisture, due to warming-induced increases in evaporative demand and decreases in precipitation, accelerates wildfire activities.[14] Seasonality of temperature and precipitation, related to latitude and to major atmospheric circulation features such as monsoons and orographic features, also plays a key role in wildfire dynamics via effects on fuel amount and seasonal fuel moisture, as in the example of seasonal high temperature and low precipitation in Australia.[15] Wind speed (W; m s^{-1}) plays a key role in fire spread, but on a global scale, its influence on BA is limited[16] (or at least wind-speed data are of insufficient quality to evaluate its effects at the global scale). Although warmer climate and drying fuel are projected to increase future BA across many regions,[8] and notably in some boreal areas,[17] empirical analysis suggests that climatic conditions that should lead to frequent fires do not always do so[10,18], suggesting a role for other, non-climatic drivers as well.

Beyond climatic conditions, humans have shaped fire regimes for thousands of years.[1,5] The most obvious direct anthropogenic impact is by ignition, since humans currently light most fires in tropical forests, savannas, and agricultural regions.[12,19] However, humans can also affect fire behavior via active fire suppression and passive suppression via, e.g., fragmentation.[12] Overall, human activities influence fire dynamics in multiple ways, but those effects can be distilled into three main factors. These are (1) population density (POP; persons km^{-2}), and thus number of anthropogenic ignitions; (2) socioeconomic development, e.g., urbanization, described as the ratio of rural to total population (RUR) (higher rural population is a major source of pyrogenic activity with longer contact with flammable vegetation); and (3) combined fire suppression and management, a proxy being the distance to human settlements (cities) (DIS; km), which is also strongly dependent on urbanization.[20] Details of the three variables POP, RUR, and DIS are given in experimental procedures, while how these human activities influence BA is described in Note S1. Continued global population growth could thus potentially increase anthropogenic ignitions[21] or alternatively decrease ignitions and suppress fires if people concentrate in cities, converting wildlands to urban areas and decreasing rural anthropogenic pyrogenic activity.[22]

An important manifestation of urbanization in the coupling of wildfire and human activities is a rapid growth of the wildland-urban interface (WUI), leading to a shorter DIS. For instance, the land area of the WUI increased in the United States by 33% between 1990 and 2010, making it the fastest growing land cover type and resulting in a significant increase in wildfire risk.[23] Worldwide, the WUI is increasing people's proximity to natural vegetation, including many protected areas.[24] Therefore, the estimation of global fire risk must account for changes in the WUI (here, via DIS; see experimental procedures), as this is crucial for modeling the long-term coexistence of socioeconomic systems and wildfires.[4] Urbanization can increase BA, as increasing numbers of people in cities and accessibility of vegetation in the WUI results in an increase in potential human ignitions.[25,26]

However, urbanization is potentially a "double-edged sword" in its effects on wildfire dynamics.[25] Although urbanization increases potential human ignitions, urbanization also brings settlements into closer proximity to potential wildfires, leading to more active wildfire suppression and management to avoid risks to health, homes, and businesses,[27] and thus decreases BA.[28] In developed countries, intensive interventions are implemented as fires approach the WUI and cities, based on aerial observation of ignitions, followed by deployment of fire retardants.[4,29] As the WUI grows, fire suppression expenditures are at an all-time high (e.g., >$1 billion annually in the United States[30]). Elsewhere, preventive measures in the form of firebreaks or managed fires are often preferred, especially where expensive interventions may not be possible, such as for much of Africa.[31] Such preventive measures have a particularly long history, for example, they are known to have been employed in the pre-Columbian Amazon.[32] In the future, Latin American and African countries are planning to implement more extensive government-controlled fire suppression, already underway in Brazil.[33,34]

The net effects of these changes in human demographic processes for fire distributions are not well understood. Recent known trends in urbanization and suppression methods provide an opportunity to test the capacity of fire models to respond to human drivers. Models should replicate both combined fire suppression and management activities that shorten potential fire duration near settlements and effects of human populations on ignitions. Human forcings do not operate in isolation and may depend on complex interactions between human societies, climate, and vegetation[5,35], such that characterizing interactions is critical for understanding how humans affect fire regimes.

Here we project global and regional trends in BA in response to simultaneous climate change and changing human demography using a modeling approach. To do this, we used the Lund-Potsdam-Jena dynamic global vegetation model (LPJ-DGVM)[36] modified to include a process-based Socio-Economic and natural Vegetation ExpeRimental global fire model (SEVER-FIRE).[26] LPJ-DGVM uses monthly climate data and an annual atmospheric CO_2 concentration as input and simulates the growth of vegetation based on an explicit description of a coupled photosynthesis-water balance scheme, with further allocation of carbohydrates to plant tissues. The model determines the competition between individuals of different vegetation types and includes accounting for plant mortality and establishment. Necromass enters the litter pool and can be either decomposed or consumed by wildfire depending on tissue dryness and surface temperature. LPJ-DGVM is considered to be one of the top state-of-the-art DGVMs and was successfully applied at global and regional scales to simulate vegetation distribution[36] and related terrestrial carbon and water cycles.[37–39] SEVER-FIRE provides a quantitative and spatially resolved global evaluation of recent historical and climate-change-driven BA trends for terrestrial ecosystems globally. SEVER-FIRE is a global fire model operating at a daily time step (here interpolated from monthly climate input within LPJ), derived from the first process-based large-scale Regional FIRe Model (Reg-FIRM).[20] SEVER-FIRE simulates all stages of wildfire development, namely: (1) fire weather risk, which depends on input climate, fuel availability, and its type (data obtained either from observations or as an output

Table 1. Experimental scenarios

Scenario	CO_2 emission scenario	Socioeconomic scenario		
		POP	RUR	DIS
S1	RCP2.6	SSP2 (middle)	SSP3 (slow)	SSP3 (slow) × *coef*
S2	RCP4.5	SSP5 (slow)	SSP2 (middle)	SSP2 (middle) × *coef*
S3	RCP6.0	SSP2 (middle)	SSP2 (middle)	SSP2 (middle) × *coef*
S4	RCP8.5	SSP3 (rapid)	SSP5 (rapid)	SSP5 (rapid) × *coef*

Overview of the experimental CO_2 emission and socioeconomic scenarios used in this study.
coef, ratio of urban area growth rate to urban population growth rate. Slow, middle, and rapid under POP mean the general levels of population growth rate, while under RUR and DIS, they mean urbanization rate.

of a DGVM), three characteristics that jointly determine fire seasonality; (2a) lightning ignition, which is determined by atmospheric convection extent and fuel type, and/or (2b) human ignition, which depends on human POP, wealth status, rural/urban ratio, and fuel type, provided as an input (see the detailed description of the influence of human factors on BA in Note S1); (3) fire spread, which is determined by climate data and fuel amount and its moisture status, as provided from observations or from a DGVM; (4) fire termination due to rainy conditions or to suppression because of proximity to human settlement (see the detailed description of the influence of human factors on BA in Note S1); and finally (5) fire vegetation mortality and carbon emissions estimated by vegetation type, again available either from observations or from a DGVM. SEVER-FIRE simulates the number of fires, the BA, and fire-related vegetation mortality and carbon emissions, which can be further used by feeding back into a DGVM or an Earth system model (ESM). The model was extensively validated at regional (e.g., Spain, Canada, and Africa) and global scales using fire statistics and remote-sensing data for both number of fires and BA.[26]

We first ran LPJ-DGVM–SEVER-FIRE (LPJ-SEVER), forced with observed climatology, over the 20th century to evaluate model performance in reproducing present-day trends in BA. We then coupled LPJ-SEVER to a computationally efficient climate emulator called Integrated Model Of Global Effects of climatic aNomalies (IMOGEN).[40] IMOGEN[40] is a computationally efficient climate emulator based on a pattern-scaling approach. Here a unique pattern (i.e., a gridded map of change in climate variables per unit global temperature change) is derived for each near-surface climate variable and ESM. Global temperature change, in turn, is modeled as a function of changing historical and future levels of atmospheric greenhouse gas (GHG) concentrations, and again calibrated against ESMs. IMOGEN can then be used for any set of CO_2 concentration or emissions scenarios (the latter including climate-carbon cycle feedbacks), to generate climate forcing for the host vegetation model (e.g., LPJ-SEVER). In this framework, wildfire-induced changes in terrestrial carbon storage can feed back to climate itself via updated atmospheric CO_2 concentration. The pattern scaling and the global warming response to rising GHGs are calibrated against 34 different ESMs (see experimental procedures) in the Coupled Model Intercomparison Project Phase 5 (CMIP5) ensemble. IMOGEN also maps from ESMs onto a common spatial grid of resolution 3.75° longitude × 2.5° latitude. Furthermore, IMOGEN predicts changes in climate, i.e., anomalies, and these are added to the University of East Anglia Climate Research Unit (CRU) climatology,[41] thus also bias-correcting ESM offsets. IMOGEN takes in monthly data and gives monthly data to LPJ-SEVER, which disaggregates to daily steps (i.e., the coupled model was operated 34 times to emulate the same number of ESMs), but all on the common IMOGEN spatial resolution of 3.75° longitude × 2.5° latitude for the period 1860–2100. We performed 34 × 4 coupled model runs in the future under four different CO_2-socioeconomic scenarios (i.e., 34 ESMs emulated × 4 scenario simulations; see experimental procedures). The four scenarios were based on four standard Intergovernmental Panel on Climate Change Fifth Assessment Report (IPCC AR5) Representative Concentration Pathways (RCPs)[42] of potential scenarios of atmospheric GHG emissions in combination with three demographic Shared Socioeconomic Pathways (SSPs)[43] (i.e., each RCP scenario is initially aligned to a specific SSP combination; Table 1, and experimental procedures). The observed CO_2 emission and human drivers were used for the historical period (i.e., 1860–2005), before divergence from present day to the end of the 21st century, due to different ESM-based estimates of climate change and different RCPs and SSPs. Validation of the model was conducted in two steps (see experimental procedures). First, we evaluated the ability of the model to reproduce recent trends in both global and regional BA against two satellite-based BA products. The first product is the Global Fire Emissions Database version 4 product including small fires (GFED4s), which is a hybrid approach combining both satellite and modeling. GFED4s was primarily produced from the Moderate Resolution Imaging Spectroradiometer (MODIS) Collection 5.1 MCD64A1 BA product and active fire data. A "small-fire boost" algorithm was used to estimate the small-fire BA from MODIS active fire detections, but this methodology may cause significant errors.[44] These measures provide global monthly BA, including the impact of small fires, at 0.25° spatial resolution from year 1997 onward.[3] The second product is the European Space Agency Climate Change Initiative BA product version 5.1 (FireCCI51), which was generated from the MODIS satellite imagery. FireCCI51 provides monthly global BA at a degraded resolution of 0.25°, starting from year 2001.[45] Second, we performed a comprehensive validation of the underlying dynamic global vegetation model itself using the International Land Model Benchmarking (ILAMB) system. ILAMB tested the LPJ model for a wide range of land carbon and hydrology cycle variables and climate forcings, all against *in situ*, remote-sensing, and reanalysis datasets.[46] In addition, we evaluated the simulated vegetation distribution by LPJ model with the latest remote-sensing-based land-cover map.[47]

We explored the dominant limiting factors, including interactive effects, on the present-day BA trend for the period 1987–2016

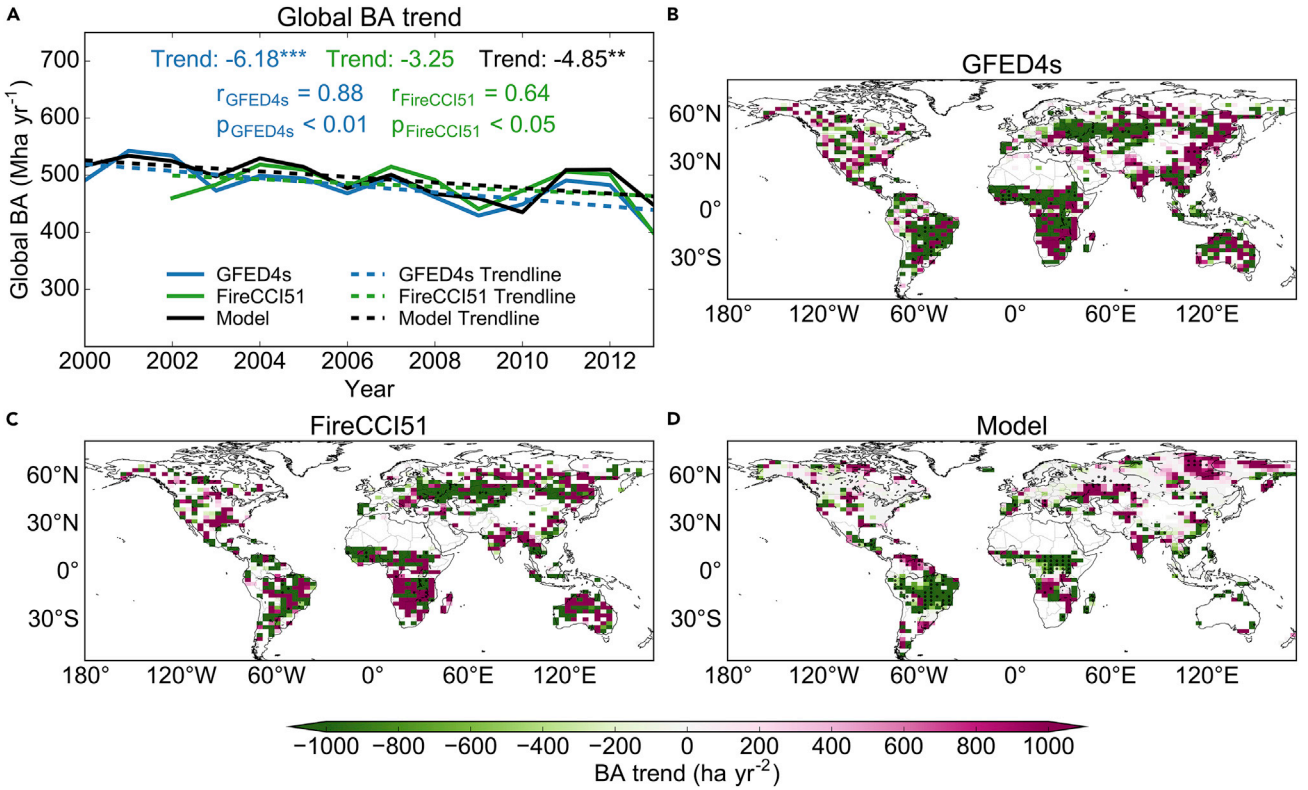

Figure 1. Present-day global BA trends

(A–D) (A) Global BA and BA trends over the period 2000–2013. Model means the global BA simulated by SEVER-FIRE driven by CRU/NCEP-observed climatology (see experimental procedures), GFED4s means GFED4s-observed BA product, and FireCCI51 means FireCCI51-observed BA product. The asterisks in this and subsequent figures indicate whether the BA trend is statistically significant (Mann-Kendall test; ***$p < 0.01$, **$p < 0.05$). $r_{GFED4s/FireCCI51}$ and $p_{GFED4s/FireCCI51}$ in this and subsequent figures represent the Pearson correlation coefficient and the p value between the simulation and the GFED4s/FireCCI51 products, respectively. The BA from FireCCI51 starts from year (yr) 2002. Spatial patterns of BA trends over the period 2002–2013 observed from (B) GFED4s and (C) FireCCI51 and simulated by (D) SEVER-FIRE are shown. Regions labeled with black dots in this and subsequent figures indicate trends that are statistically significant (Mann-Kendall test; $p < 0.05$).

using model factorial simulations. Factorial simulations can isolate the impact of individual factors by fixing one variable at a time (either a climatic variable, T, P, and W, or a socioeconomic variable, POP, RUR, and DIS). These six factorial historical runs enabled mapping of the limiting extent of each factor and calculating its importance as the sum of the number of grid cells with the same dominant limiting factor divided by the total number of global burned land grid cells. We also projected the future global BA trends over the period 2014–2100 and analyzed simulated spatial patterns and drivers using a partial derivatives approach by varying one driver at a time, yielding six runs over the last 30 years of the 21st century (see experimental procedures). Finally, to clarify the relative importance of future human impacts on BA dynamics, a sensitivity analysis was performed exploring all combinations of population growth and urbanization rates, where the latter determined the evolution of DIS and RUR.

RESULTS

Present-day global BA trend

Fire dynamics simulated in "offline mode" were validated against satellite-based GFED4s and FireCCI51 observations, suggesting a reasonable match between modeled and observed temporal trends in recent global BA (Pearson correlation analysis, $r = 0.88$, $p < 0.01$ and $r = 0.64$, $p < 0.05$, respectively; Figure 1A). Overall, when driven by observed climatology, SEVER-FIRE yielded decreasing BA at a rate of −4.85 Mha year^{-2} over the period 2000–2013 (Mann-Kendall test, $p < 0.05$), thus successfully reproducing recent negative global BA trends of −6.18 Mha year^{-2} in GFED4s and −3.25 Mha year^{-2} in FireCCI51 (Mann-Kendall test, $p < 0.01$, $p = 0.45$, respectively; note that FireCCI51 covers only 2002–2013). Regional evaluation in observed against simulated recent BA trends, mean annual BA, temporal correlation, and spatial correlation of grid-cell-based BA dynamics showed that our model broadly captured the major pattern of the observed BA (Note S2). Generally, the simulated spatial pattern of the trends in BA compared well with the satellite-based GFED4s and FireCCI51 products (Figures 1B–1D). The model captured observed negative trends across central South America, mesic African savannas, Southeast Asia, western Europe, and the northern Australia and positive trends around western Canada, California, parts of northern Eurasia, and South Asia over the period 2002–2013. However, there are still large uncertainties and biases in recent simulated-against-observed BA

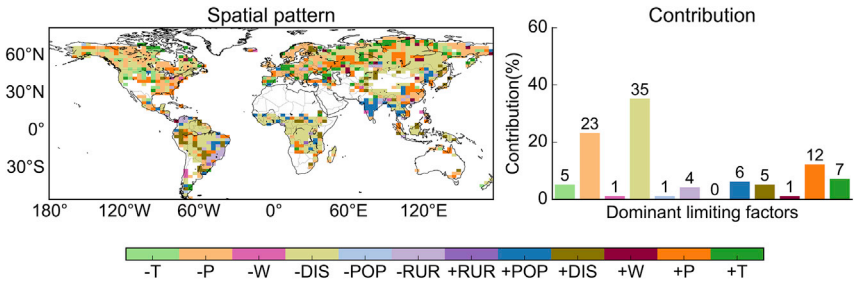

Figure 2. Attribution of dominant limiting factors of spatial patterns of present-day BA trend over the period 1987–2016

Bar plots (right) indicate the fraction of global burned land grid cells (%) where changes in BA trend are attributed to different dominant limiting factors. The legend is provided as a set of rectangular labels at the bottom. The prefix "+" means that a change in a limiting factor has a positive impact on BA trend, whereas "−" means that a change in a limiting factor has a negative impact on BA trend. T, temperature; P, precipitation; W, wind speed; POP, population density; RUR, ratio of rural to total population; and DIS, average distance from the nearest city.

trends (Note S2), even between GFED4s and FireCCI51 (see, e.g., diverging trends in eastern China and the Brazilian Cerrado and Caatinga). Comprehensive validation of LPJ-SEVER using the ILAMB system, including an assessment of the global vegetation distribution, is provided in Note S3.

Limiting factors of present-day BA trend

Recent BA changes were influenced by a range of factors.[48] Although these interacted, factorial simulations can nevertheless help to attribute the dominant limiting factors to BA trends.[49] At a global scale, over the period 1987–2016, factorial simulations suggest that present-day BA trend was predominantly limited by DIS (km) on 40% of global burned land grid cells, followed by climate factors, including P (mm) (35%), T (°C) (12%), and W (m s^{-1}) (2%), with 11% attribution to other socioeconomic factors (POP [persons km^{-2}] and RUR) (see Figure 2). Overall, climate (as the sum of T, P, and W) and human activity (as the sum of DIS, POP, and RUR) were equally limiting to present-day fire activity (49% and 51% of the global burned land grid cells, respectively; Table S5). The effects of DIS, representing combined human fire suppression and management, were most limiting of trends in areas with frequent fires in South America, central Africa, Alaska, Southeast Asia, and northeast China. Climate, in particular T and P, was most limiting in Northern Hemisphere high-latitude areas and in places that are already heavily urbanized (where additional urbanization is unlikely to affect trends), including Europe and the eastern United States.

Future BA trend projection

We projected future global BA trends, represented as ensemble means across 34 ESM-based IMOGEN-LPJ-SEVER simulations (i.e., an integrated BA after 34 independent runs), under four experimental scenarios, S1 to S4 (Table 1). These four ensemble means corresponded to the period 2014–2100. The strong mitigation scenario S1 resulted in a slightly negative BA trend (−0.03 Mha $year^{-2}$) via low emissions, intermediate population growth, and slow urbanization; the typical mitigation scenario S2 in a large negative BA trend (−1.69 Mha $year^{-2}$; Mann-Kendall test, $p < 0.01$) via slow population growth; and the intermediate mitigation scenario S3 in a smaller negative trend (−0.58 Mha $year^{-2}$; Mann-Kendall test, $p < 0.01$) via intermediate population growth. However, we found a significant increase in BA in response to S4, currently the "business-as-usual" scenario with high emissions, rapid population growth, and rapid urbanization (0.88 Mha $year^{-2}$; Mann-Kendall test, $p < 0.01$) (Figure 3A).

To understand climate and human factors limiting future BA change, we conducted a set of factorial analyses using the S3 scenario for three ESMs covering a range of future global P changes for the period 1860–2100 (see experimental procedures and Note S4). Combined anthropogenic fire suppression and management (via proximity to city settlements, DIS) was a major factor limiting potential growth of global BA driven mainly by exponential population growth (Note S4). To illustrate, under the intermediate mitigation scenario, a constant DIS (set to the size of the DIS in 1950) would result in a BA at the end of 21st century almost three times larger than that projected with realistic change in the DIS; this demonstrates the strong suppressive effect of urbanization on BA (Figure 3B). A sensitivity analysis using the RCP6.0 CO_2 emission scenario (Table 1) covering the range of possibilities in population growth/urbanization rates showed that, for a rapidly growing population, urbanization tended to decrease global BA (Figure 3C).

The spatial patterns of ensemble mean BA trends across 34 ESM-based IMOGEN-LPJ-SEVER simulations for four scenarios, S1 to S4 (Table 1), over the period 2071–2100 are shown in Figure 4. The results show large differences among the scenarios. Scenario S1 resulted in a significant negative trend globally (−1.78 Mha $year^{-2}$; Mann-Kendall test, $p < 0.01$; inset of Figure 4A), with large declines in BA in the Amazon, mesic African savannas, Siberia, and South Asia. Scenario S2 also showed a significant negative trend globally (−2.39 Mha $year^{-2}$; Mann-Kendall test, $p < 0.01$; inset of Figure 4B), but with positive trends in North America (excluding Alaska) and western Europe compared with S1 (Figure 4B versus 4A). Scenario S3 showed patterns similar to S1 and S2, except that BA was projected to increase across the Amazon, and Siberia was relatively unchanged (Figure 4C; overall global BA trend of −0.59 Mha $year^{-2}$; Mann-Kendall test, $p < 0.05$). Scenario S4 instead showed a significant positive trend globally (2.18 Mha $year^{-2}$; Mann-Kendall test, $p < 0.01$; inset of Figure 4D), focused across the Amazon, northwest Eurasia, and Southeast Asia (Figure 4D).

Drivers of future BA trend

We estimated the contributions of three climatic (T, P, and W) and three socioeconomic factors (POP, RUR, and DIS) to BA trends for 2071–2100 by fixing all but one factor at a time. The dominant drivers of regional BA trends in the future were climate change and changes in POP, with the magnitude of their contributions varying with emission-socioeconomic scenario (Figure 5 and S10). For scenario S1 (lowest emissions, middle population

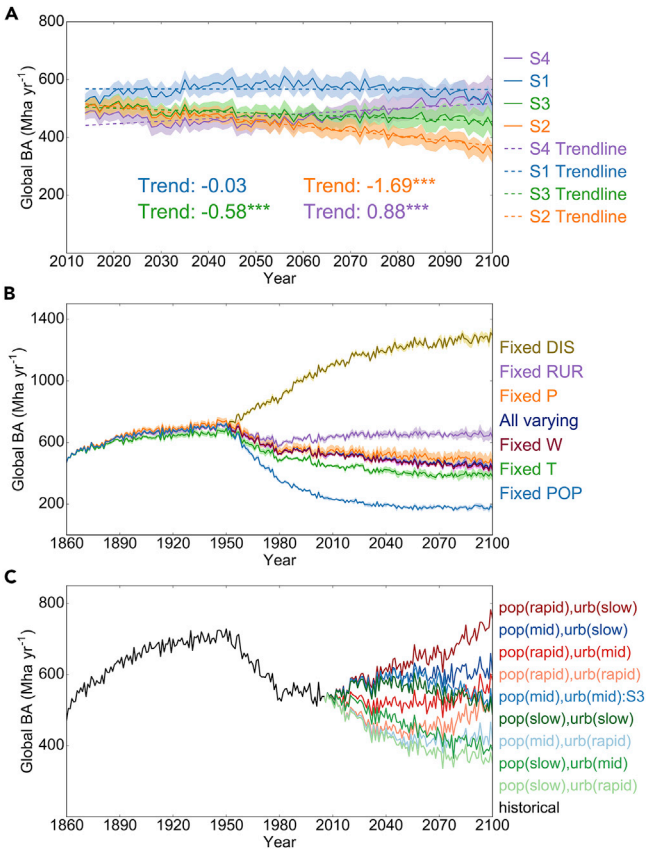

Figure 3. Projected global BA trends

(A) Future BA trends over the period 2014–2100 using four experimental scenarios (Table 1). The shaded areas represent the standard deviation for the results of 34 runs. ***$p < 0.01$ (Mann-Kendall test).

(B) Factorial analysis on long-term global BA in the S3 scenario (Table 1) over the period 1860–2100. The shaded areas represent the standard deviation for the results of three ESMs (see experimental procedures). T, P, W, POP, RUR, and DIS are the same as those in Figure 2.

(C) Sensitivity analysis under RCP6.0 CO_2 emission scenario by exploring all combinations of population growth rate (pop) and urbanization rate (urb) from SSPs. "mid" represents "middle" in Table 1 and "S3" represents the S3 scenario in Table 1.

growth, and slow urbanization), climate change was mild, and POP was the dominant driver of changes in BA in most tropical and subtropical regions, and BA changes in northwestern Russia were dominantly driven by urbanization (Figures 5A and S10A). For scenario S2 (second lowest emissions, slow population growth, and medium urbanization), regional BA changes tracked decreasing population trajectories in South America, tropical Africa, Southeast Asia, and Russia, with increasing BA tracking population increases in Europe and North America. Changes in geographic BA trend distribution were explained mainly by the SSP5 demographic scenario.[50] Climate effects (mainly of temperature) were concentrated in high latitudes and mountain areas (Figures 5B and S10B). For scenario S3 (second highest emissions, medium population growth, and medium urbanization), climate change was more severe, and therefore the influence of climate drivers (sum of T, P, and W) on global BA trends also increased (globally, 47% of global burned land grid cells were dominated by climate drivers in scenario S3 compared with only 29% for scenario S2; Figures 5B and 5C). Climate effects due to temperature were no longer restricted to Russia, Scandinavia, and North America (where population change was minimal), but extended also into the Amazon and East Africa due to changes in precipitation (Figure 5C). Finally, for the most extreme scenario, S4 (highest emissions, rapid population growth, and rapid urbanization), although human-induced fires were important over the tropics and subtropics, climate determined 52% of the global BA trend, due to high latitude warming (in, e.g., Russia and Canada) and to tropical and subtropical drying (Figures 5D and S10D). Regionally, changes in BA over the Amazon rainforest were driven predominantly by population growth and precipitation changes. Generally, decreasing precipitation across the Amazon over the last 30 years of this century increased BA (Figure S11), although some years with increased precipitation also contributed (Figure 5D). This demonstrates how increased precipitation can operate in two competing ways, by increasing BA due to increased vegetation growth and thus more fuel or, alternatively, by decreasing BA through increasing moisture levels in fuel. In addition, there existed possible compensatory effects going from the local scale to the global,[51] i.e., although globally, changing population distributions remain important (Figure 5 and Note S4), climate change compensates locally (Figure S10).

DISCUSSION

Here, we present results of a global fire model that reproduced a negative global BA trend observed in GFED4s and FireCCI51 over the recent historical period,[5] which suggests a reasonable representation of fire responses to climate and human activity in SEVER-FIRE.[26] Effects of human activity are the major innovation of the model, with mechanisms based primarily on fire termination (using DIS as a proxy for speed of suppression) and ignitions (dependent on POP and ratio of rural population). Spatial patterns of simulated trends in BA were generally consistent with studies showing recent declines in BA in the tropical savannas of South America[52] and Africa.[5,7,53] In our model, declines are driven by rural-urban transformation (included explicitly) and by agricultural commercialization, diversification of economic activities, and increase in property size (implied in model mechanisms). Although economic transitions and associated land-use and land-cover change are not formally modeled, key aspects are implied via changes to wildfire activity in both urban and rural areas as wildland is urbanized.[54] The model assumption that wealth is not changing in abandoned rural areas leads to increases in the sizes of individual land owners' properties, similar to the conceptual model of Andela et al.[5] This has the effect of causing decreases in ignition activities related to a smaller number of ignition agents and changes in the timing of pyrogenic activities, both of which result in a decrease in BA. However, the model underestimates BA in North America; total BA may be underestimated because of either issues with estimating lightning ignitions[2] or some aspect of fire duration and extinction[12] (a known limitation of fire models generally).

The models that reproduced historical BA trends also enabled predictions of future BA trajectories. For milder atmospheric GHG emissions scenarios (scenarios S1–S3 in Figure 3A), our

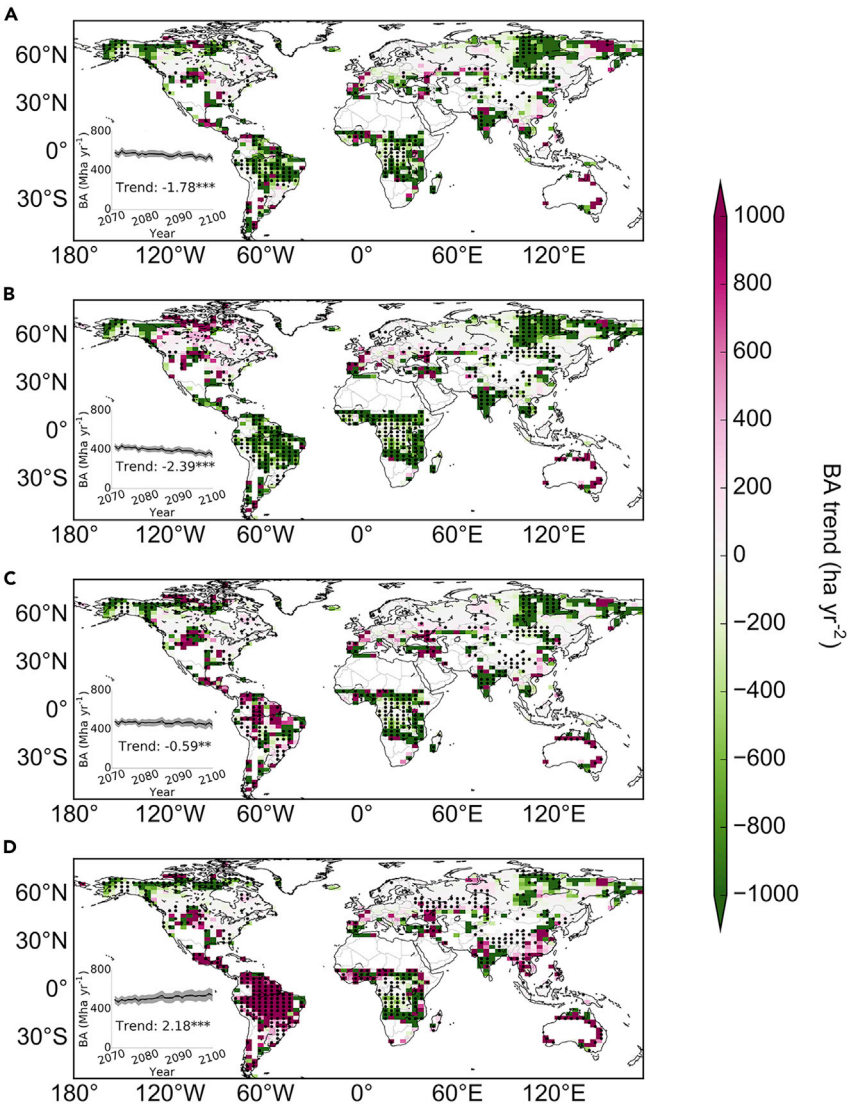

Figure 4. Spatial patterns of future BA trends

Shown are the ensemble mean BA trends across 34 ESM-based IMOGEN-LPJ-SEVER simulations over the period 2071–2100 for the four scenarios listed in Table 1. (A) S1, (B) S2, (C) S3, and (D) S4. Line plots (inset) indicate global BA trends for the same period, and the shaded areas represent the standard deviation for the results of 34 runs. ***$p < 0.01$, **$p < 0.05$ (Mann-Kendall test).

model predicted declining global BA. By contrast, with the highest emissions and rapid population growth and urbanization (scenario S4 in Figure 3A), global BA instead increased, driven by population growth and by drying in tropical and subtropical areas and warming and drying over high latitudes and mountainous areas. The largest difference in BA trends among scenarios occurred during the period 2071–2100 across central South America, including the Amazon, and in northern Eurasia, including Siberia (Figures 4A–4D). Rapid population growth and precipitation changes were projected to lead the Amazon to change into a fire-prone ecosystem, whereas warming alone led to increases in BA across northern Eurasia (Figure 5D). Under scenario S4, warming, drying, and population growth combined to dramatically increase BA globally (see also Knorr et al.[10]). The effects of climate were particularly obvious across high-latitude regions, where temperature was a dominant driver across 36% and 38% of global burned land grid cells under scenarios S3 and S4, respectively (Figure 5).[14,55,56] Future research could include millennium-scale analyses, capturing longer time scales of global temperature responses to emissions. For instance, even if emissions reduce to zero after year 2100, global temperatures will continue to be raised for many centuries (e.g., Eby et al.[57]). Long-term warmer, and possibly drier, conditions may lower fuel availability in tropics/subtropics due to the associated decrease in vegetation productivity and readjustment of spatial patterns of vegetation distribution. Therefore, while an increase in BA is seen under scenario S4 in the last 30 years of the century, global and regional BAs may start to decrease in a long-term period after 2100. In addition, carbon cycle/vegetation cover may also be slow, with transient dynamics that dominate in the near term, approaching a new equilibrium after 2100.[37,58]

Drivers of BA trends are likely to change substantially in the future, but whether they affect the BA response will also depend on the other limiting factors operating at any given time. The overall BA trends were also strongly limited by proximity to human settlements (DIS) across 47%–54% of global burned land grid cells in all four scenarios (Table S5 and Figure S12), consistent with the idea that the intensity of fire suppression and management increases with proximity to settlements.[10] Our sensitivity analysis covered the range of possibilities in population growth and urbanization and suggested that, where population growth is rapid, faster urbanization will decrease BA (Figure 3C). Urbanization thereby offsets potential dramatic increases in global BA resulting from changing climate and population growth (Figure 3B and Note S4). However, despite the appearance of new frontiers of fire suppression near new and growing cities, an enhanced wildfire-human settlement interface was insufficient to fully offset other climate and socioeconomic factors, as evidenced by the fact that, despite urbanization, extreme CO_2 emissions scenarios led to general increases in BA. Moreover, rapidly developing countries (e.g., Brazil, Russia, India, and China) were projected to be major contributors to future global BA for both climatic and anthropogenic reasons (Figures 4 and 5); future changes in fire suppression and management in these countries could strongly influence global BA trends.[59–61]

Our results highlight the global importance of fire suppression for recent and future fire regimes and suggest how the

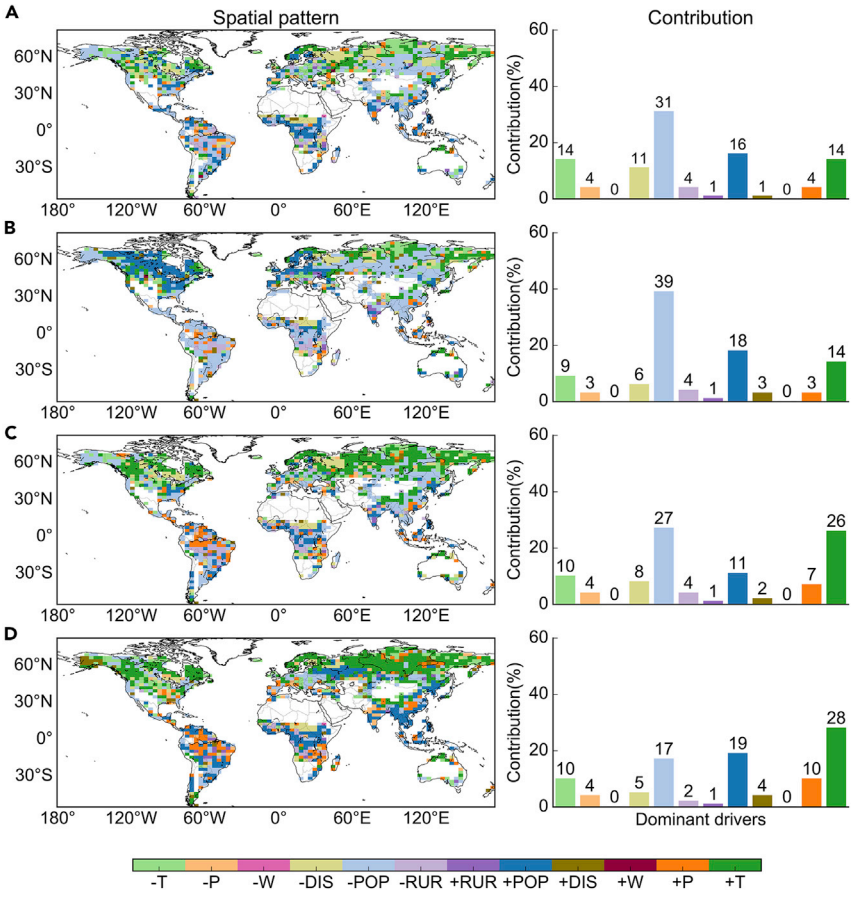

Figure 5. Attribution of dominant drivers of spatial patterns of future BA trends over the period 2071–2100

Shown are the four scenarios listed in Table 1. (A) S1, (B) S2, (C) S3, and (D) S4. Bar plots (right) indicate the fraction of global burned land grid cells (%) where changes in BA trend are attributed to different dominant drivers. The legend is provided as a set of rectangular labels at the bottom. The prefix "+" means that a change in a driver has a positive impact on BA trend, whereas "−" means that a change in a driver has a negative impact on BA trend. T, P, W, POP, RUR, and DIS are the same as those in Figure 2.

human aspects of fire regimes (including fire management) can sometimes change historical fire-weather relationships. For instance, in southern France, starting in the 1990s, fire suppression decreased the number of fires ignited by the same weather conditions.[62,63] However, the probability of strong winds has concurrently increased, resulting in fire activity that is dominated by hot, windy weather, instead of by fuel moisture. Thus, despite fire suppression, BA is predicted to increase by 30% by the end of the century (2071–2100) in the Mediterranean under the RCP8.5 scenario,[64] a prediction that parallels scenario S4 in our study. This interaction of fire suppression with weather is not included in our model, however, and may potentially exacerbate predictions: declines in BA for the low emissions scenarios (S1–S3) may be stronger than projected, whereas increases in BA in the high emissions scenario S4 may be even amplified, if the interaction of weather and fire suppression leads to larger fires.[64] The next generation of global fire models incorporated into DGVMs/ESMs should account for the impacts of fire suppression on the observed relationship between fire and weather.[62] New fire models should also capture the existence of ecologically or economically optimal fire suppression strategies proven to be effective[65,66] and should also account for conditions leading to extreme but rare "firestorms" that contribute substantially to BA. All of these factors will enable more accurate estimates of global and regional dynamics of BA.

In the fire modeling literature, the issue of BA trends and their drivers remains controversial.[6,7,9,10,67] Here our results provide potential insights into why published models diverge in their predictions: they stem mainly from regional differences in BA trends and the alternative representation of mechanisms of fire occurrence, spread, and termination within fire models. Most studies suggest an increasing BA trend[7–9], especially in the last three decades of 21st century[6,67], consistent with our finding that, under severe climate change and population growth scenarios, BA is likely to increase, especially in places subject to intense warming and drying. However, we also projected negative global BA trends in three of four future scenarios, limited primarily by changes in fire suppression and management associated with urbanization. This is consistent with a smaller literature arguing that, globally, BA trends are likely to be heterogeneous[8] and to depend on human demographic factors.[10] SEVER-FIRE extends previous analyses[10] by improving descriptions of pyrogenic human behaviors, e.g., prescribing different timing of ignitions for rural and urban populations.[26] We also take into account the feedbacks between vegetation, humans, wildfires, and the climate system by using a coupled online framework, extending past work with focused instead of linear responses.[10] This coupled framework allows for a dynamic response of ecosystems to changing fires and for feedbacks between changing atmospheric conditions and fire behavior. These innovations result in a wide divergence of non-linear responses of global BA to POP and urbanization changes (Figure 3C).

Despite these improvements, however, here we consider the effects of only relatively coarse-grained demographic variables on fire behavior and BA. In reality, the influences of human activities on fire dynamics are likely to be more complicated than this. Their representation in models may need to include agricultural production, explicit consideration of fire management, land-use and land-cover change,[12,21] fragmentation,[68] and even complex interactions among social and ecological systems.[69] Human activities can also have complicated seasonality: here, we prescribe the timing of rural ignitions to align with the timing of major agricultural seasons (spring and fall), which allows us to simulate how

agricultural fires escape to influence wildfires (e.g., Spain[20]). However, explicitly representing agricultural management fires as separate from wildfires may be another useful step for future work. Deliberate agricultural fires account for ~10% of global fires,[70] but they have different seasonality, frequency, and intensity in comparison with wildfires. Furthermore, Korontzi et al.[70] show that fire regimes for agricultural fires are highly dependent on regional agricultural practices, types of crops, and yield output. Thus, the implementation of simulated agricultural fires into ESMs requires well-developed descriptions of expected pyrogenic activity of farmers around the globe. Population density today at a global scale shows a strong negative relationship with recent BA change largely due to landscape fragmentation and fuel reduction,[21] which could be simulated in our coarse resolution study only implicitly by implementing urbanization. Moreover, recent BA trends in Africa may have been driven by cropland expansion over the period 2001–2012;[71] we can only peripherally address this by providing an improved map of projected global BA distribution after integrating cropland impact (Note S2), which confirms the potential influence of land-use change on BA. However, it is also clear that human effects on fire regimes merit greater and more diverse research emphasis, examining land use, especially crop versus pasture expansion, and abandonment of culturally traditional burning.[72] Other variables, too, may merit examination; for example, roads and power lines are not represented in most global models but may play important roles as ignition sources or firebreaks.[22] Their role in global fire regimes now and in the future can be assessed only by coupled models with sophisticated socioeconomic descriptions. Moreover, the effects of other factors, like lightning,[2] CO_2 fertilization[10] (via resprouting of adaptive trees in semi-arid regions),[73] and fuel load and fuel availability,[48] on BA changes deserve further study.

In summary, we show that the historical global BA has decreased, notably for central South America and mesic African savannas, and formulate a new model that reproduces trends well, capturing recent climate and human limits on changes in BA. This model projects divergent trends in the future, depending on climate and socioeconomic scenario. Under severe climate change scenarios, fire activity increased, largely due to accelerated high-latitude warming and tropical and subtropical drying. However, human activities were important even in severe scenarios, and dominated the BA signal in milder scenarios. Urbanization in particular strongly shaped patterns; active and passive fire suppression in the vicinity of human settlements was important in offsetting large potential BA increases. Overall, understanding both the climatic and the human controls on long-term BA trends is a first, yet critical, step toward better projections of the future of wildfire in a changing climate.[4]

EXPERIMENTAL PROCEDURES

Resource availability

Lead contact

Further information and requests for resources should be directed to and will be fulfilled by the lead contact, Chao Wu (chaowu.thu@gmail.com).

Materials availability

This study did not generate new unique materials.

Data and code availability

All data used to evaluate the conclusions of the paper and generate the figures and tables are available at https://doi.org/10.6084/m9.figshare.14256272. The Python codes to interpret data and prepare the figures are available on request from the lead contact. GFED4s is available at http://www.globalfiredata.org/index.html. FireCCI51 is available at https://geogra.uah.es/fire_cci/firecci51.php. ILAMB is available at https://www.ilamb.org/. National Centers for Environmental Prediction (NCEP) Reanalysis data were provided by the NOAA/OAR/ESRL PSD, Boulder, Colorado, USA, from their website at https://www.esrl.noaa.gov/psd/. The IMOGEN model and the latest version are available from C.H. (contacted at chg@ceh.ac.uk).

Model

LPJ-DGVM–SEVER-FIRE (LPJ-SEVER)

A process-based global fire model (SEVER-FIRE),[26] which was developed from Reg-FIRM,[20] used for reproducing and projecting future global BA and its trends, was coupled to LPJ-DGVM.[36] Reg-FIRM was used in previous regional human-dominated ecosystems: Iberian Peninsula fire regime reproduction.[20] However, the structure and the parameterization oriented to the global scale of the fire model have been updated in SEVER-FIRE.[26]

One of the major novelties of SEVER-FIRE is an implementation of the pyrogenic behavior of humans (e.g., differential timing of contact with vegetation within a year), which provides additional spatial and temporal variation in BA trends due to different fire weather conditions for urban and rural population-induced ignitions.[26] Overall, increasing numbers of people in cities and accessibility of vegetation in the WUI may result in an increase in potential human ignitions,[25,26] although under high population densities, fire activity may decrease due to proximity to suppression resources.[28] An additional novel aspect of our approach is the implementation of a description, in simplified form, of combined fire suppression and management activity that, together with weather conditions,[26] determines potential fire duration. This is characterized and assumed through a proxy quantity, described by an average fire duration that increases exponentially with distance from the city borders. Based on climate forcing, external anthropogenic drivers, and LPJ-DGVM-derived vegetation (e.g., fuel state set by vegetation dynamics), SEVER-FIRE provides at the global scale a mechanistic description of major fire characteristics, namely number of fires, area burned, and fire carbon emissions, which are separated into human-induced and lightning-induced fires by their ignition sources. The post-fire conditions then regulate vegetation and ecosystem regeneration, which acts as a feedback to burning, driving conditions of new fuel load accumulation and the difference in flammability among plant functional types in the DGVM. BA has been widely used in assessing the effects of fire.[1,11,74] More details of the description of SEVER-FIRE can also be found in Venevsky et al.[26]

The IMOGEN climate-carbon cycle system

LPJ-SEVER is forced by a common base climatology plus patterns of changing meteorological conditions fitted against the 34 CMIP5 ESMs (Note S3). "Pattern scale," which approximates linear relationships found between local and seasonal meteorological variation and the amount of global warming over land,[75] is used to calculate climate change.[40,76,77] An energy balance model calculates global warming amounts from changes in atmospheric GHGs, also fitted to the CMIP5 ensemble. This component is coupled to the LPJ-SEVER with vegetation dynamics, which provides land-atmosphere feedback via the net biome production flux. This flux is calculated as integrating grid-box mean values of net primary production minus heterotrophic respiration and fire carbon emissions. A simple global oceanic model gives ocean feedback to the atmosphere by the oceanic drawdown of CO_2.[40] This combined impact system, IMOGEN, is operated online with a closed carbon cycle and thus forced with anthropogenic CO_2 emissions. Annual CO_2 concentrations are updated at the end of each year based on annual CO_2 emissions and changes in global land and ocean carbon fluxes from LPJ-SEVER and the global ocean model, respectively.[37] Non-CO_2 GHG emissions are not considered in this study. The flowchart of the IMOGEN-LPJ-SEVER framework is shown in Figure S13.

Forcing datasets

Atmospheric composition and climate datasets

For the offline historical simulations, we used observed fields of monthly climatology for the period 1950–2016 from the University of East Anglia CRU gridded dataset,[41] supplemented by variables from the NCEP/National Center for Atmospheric Research (NCAR) Reanalysis dataset[78] (e.g., P, convective P, and W). These climate datasets were aggregated to a resolution of 3.75° longitude × 2.5° latitude through the nearest-neighbor interpolation method,

in keeping with the resolution of the climate patterns of ESMs used in IMOGEN. Meanwhile, we used annual global atmospheric CO_2 concentrations for the period 1950–2016 based on atmospheric observations during offline historical simulation.[37]

For the fully coupled online carbon-cycle simulation, IMOGEN required prescribed fossil fuel CO_2 emissions, which were based on historical records over the period 1860–2005.[79] RCP2.6, RCP4.5, RCP6.0, and RCP8.5 emissions scenarios were used for the period 2006–2100. The interannual varying climate is necessary for LPJ-SEVER to simulate realistic fire dynamics,[37] which is simulated at daily steps. Therefore, 34 patterns from ESMs were added to a random sequence of years between 1901 and 1930 from the CRU dataset.[80] Hourly surface climate was derived by temporal disaggregation of the monthly means, including T at 1.5 m, diurnal T range, P, and W, and resulting monthly T, maximum/minimum T, P, convective P, and W were used to force LPJ-SEVER.[40] The monthly climate data were interpolated to daily values within LPJ-DGVM in order to force SEVER-FIRE. However, we assumed that cloudiness fluctuation would not change with time, and the constant long-term means were used to force the model in this study.[36] All the data used in the simulation (including the socioeconomic variables in the next section) was prepared as a spatial resolution of 3.75° longitude × 2.5° latitude, in keeping with associated patterns of ESMs, and the nearest-neighbor interpolation method was used if needed.

Socioeconomic scenarios

SEVER-FIRE is also forced by socioeconomic variables, mainly including POP, RUR, and DIS. Human factors of BA variability (i.e., POP, RUR, and DIS) are non-linear in time. The relationships between these factors are changing through time according to socioeconomic scenario. The common global gridded (urban) POP base maps over the period 1950–1959 were derived from the United Nations Population Division (https://esa.un.org/unpd/wpp/Download/Standard/Population/). The following years' POP could be obtained by the annual average population growth rate multiplied by the common base map. The annual average (urban) population growth rate (%) was extracted from the SSP database,[43] which described the world's different levels of challenges to climate mitigation and adaptation.[10] SSP2 represents an intermediate scenario of middle of the road, with middle population growth and middle urbanization; SSP3 reflects rapid population growth and slow urbanization, leading to a high challenge of mitigation and adaptation; SSP5 describes a world with conventional economic growth and mounting fossil fuel consumption leading to rapid urbanization but with slower population growth.[10] The World Bank World Development Indicators' historical population annual average growth rate was used for the period 1960–2005. For the period 2006–2100, the SSP2, SSP3, and SSP5 scenarios, which were provided by the NCAR, were selected to project the potential growth rate of POP based on five different regions with different development levels.[43] Similarly, the projection of RUR for the period 1950–2100 was prepared according to urban POP baseline and urbanization speed rate. But the historical records were from World Urbanization Prospects (WUP2009).

Variable DIS, in our approach, operates as a proxy variable that combines fire suppression and management and, as expected, is strongly related to levels of urbanization. An auxiliary role of DIS is in constraining the number of human ignitions due to conversion of wildland to urban territories as the probability of ignition is set to zero, when DIS is zero in the model. Generally, global urban areas are expanding on average twice as fast as their populations,[81] as was suggested recently by power scaling relationships in cities that remain valid over many centuries.[82] However, a parameter, *coef*, defined as the ratio of urban area growth rate to urban population growth rate, varies geographically and depending on how diverse development levels are for different regions.[83] We assume that the DIS changes at the same rate as the growth of urban areas. The initial values of DIS for a grid cell (3.75° × 2.5°) for this study were recalculated from a dataset with 0.5° × 0.5° spatial resolution.[26] Values are derived as the distance from the grid cell to the nearest grid cell with a POP exceeding 400 persons km^{-2}, which was considered a threshold for an urban system[84,85] (see maps of recent and future DIS in different SSPs from Figure S14). Based on the "low projection" scenario (i.e., assuming constant urban densities) of Tables 6.1 and 6.2 in Angel et al.,[83] we calculated the ratios of urban area growth rate to urban populations (i.e., *coef*) in five regions. These correspond to the regions defined in the SSPs, and thus we obtained the growth rate of DIS and projected DIS for the historical and future period, years 1950–2100.

Experimental design

Model initialization

The fully coupled IMOGEN-LPJ-SEVER simulation started from "bare ground" (no plant biomass present) and "spun up" 1,000 years until approximate equilibrium of carbon pools and vegetation cover was reached.[36] A random sequence of years between 1901 and 1930 from the CRU dataset, the socioeconomic forcing data in the year 1950, and a constant atmospheric CO_2 concentration at preindustrial were used to force the coupled model. Meanwhile, CO_2 emissions were "switched off" and no feedbacks from land or ocean to the atmosphere were used during the model initialization.

Offline historical LPJ-SEVER simulation

In the first set of experiments, LPJ-SEVER was run from its preindustrial equilibrium over the historical period 1950–2016 using observed fields of monthly climatology CRU datasets, NCEP/NCAR Reanalysis datasets, and historical annual global atmospheric CO_2 concentration, at the ESM grid resolution of 3.75° longitude × 2.5° latitude. The input soil texture data were the same as in Sitch et al.[36] No land or ocean carbon-cycle feedbacks were included at this stage.[37]

Fully coupled IMOGEN-LPJ-SEVER simulation

LPJ-SEVER was run from its preindustrial equilibrium in 1860 over the historical and future period 1860–2100 at the spatial resolution of the ESMs' patterns. Once the equilibrium state was reached, LPJ-SEVER was run in transient mode forced by the IMOGEN framework using climate anomalies from 34 ESM patterns (i.e., the couped model was run 34 times depending on different ESMs). Climate anomalies were added to a random sequence of 30 years of baseline climatology. This was undertaken for four IPCC AR5 RCP fossil fuel CO_2 emissions scenarios (RCP2.6, RCP4.5, RCP6.0, and RCP8.5). Meanwhile, three external anthropogenic SSPs (SSP2, SSP3, and SSP5) were added to the fully coupled simulation (with socioeconomic data of year 1950 also used for the period 1860–1949 of the transient phase). The experiment scenarios are shown in Table 1.

Model validation

We validated the model in two steps. Based on "offline" historical simulation, we first evaluated the model's ability to reproduce both global and regional BA trends for the recent historical period (2000–2013) against two satellite-based BA products. These products were the GFED4s[3] and the FireCCI51[45] from the European Space Agency Climate Change Initiative. We then performed a comprehensive validation of our underpinning dynamic global vegetation model LPJ. To achieve this, we used the ILAMB system for a wide range of land carbon and hydrology cycle variables and climate forcings, all against *in situ*, remote-sensing, and reanalysis datasets.[46] Benchmarking tests were conducted for all LPJ simulations driven by (1) "offline" observed climatology and (2) climate forcing from 34 ESMs within the IMOGEN framework, and for the historical period. The results showed that our model performed well in simulating most land variables (more details can be accessed from Note S3). In addition, noting that fire has an important effect on vegetation distribution[86,87], we evaluated our simulated "offline" present-day global vegetation distribution (i.e., with fire included) by comparing it with the European Space Agency's Land Cover Climate Change Initiative dataset[47] (Note S3).

Analysis

Present-day and future BA trends projection

Based on the offline historical simulation, the present-day (the period 2000–2013) global BA and its trends were reproduced and evaluated by the satellite-based long-term BA products (i.e., GFED4s and FireCCI51). The simulated spatial pattern of present-day BA trends was compared with those from GFED4s and FireCCI51. A nearest-neighbor interpolation was used to remap the observed datasets from their original resolutions to 3.75° × 2.5°. Regional evaluations of observed-against-simulated present-day BA trends, mean annual BA, and temporal BA correlations were analyzed in 14 GFED basis regions[88] (Note S2). In addition, we used a present-day cropland map to correct projected BA by masking out BA in cropland, making the assumption that no fires occur in cropland, to better understand the role of cropland on the spatial pattern of present-day BA (Note S2). The spatial pattern of the correlation of grid-cell-based simulated-against-observed temporal BA dynamics was evaluated by a Pearson correlation analysis (Note S2). The future global BA trends were projected in four different scenarios, S1–S4 (Table 1), over the period 2014–2100. We also projected the spatial patterns of BA trends for the last

30 years of the 21st century in different scenarios to explore the spatial difference of BA trends under different emissions and demographic forcing.

A trend in BA was calculated based on a simple linear regression (Equation 1):

$$y = \gamma + \beta t + \varepsilon, \quad \text{(Equation 1)}$$

where y is the temporal BA, t is the year, and regression coefficients γ and β are obtained through the least-squares fit. ε is the residual of the regression. β is defined as the linear trend in BA. The Mann-Kendall test was used to estimate the statistical significance of the trend.

Limiting factors of present-day BA trend

Human and climatic effects are generally considered the main factors in influencing BA trend.[5,10] However, limiting factors and drivers are different. Drivers can change substantially, but whether they affect the BA response will depend on the other limiting factors operating at any given time (a schematic illustrating how limiting factors and drivers were differently defined is Figure S15). Dominant limiting factors were described as the factors that limited most to an increase (or decrease) in BA trend in each grid cell, including interactive effects among different factors (i.e., we considered the interactions between climatic and human impacts). We performed six factorial experiments in the offline scenario (Table S5) to evaluate the dominant limiting factors, namely, T, P, W, POP, RUR, and DIS, on present-day BA trends: F1, fixed T using non-varying T of the year 1950; F2, fixed P using non-varying P of the year 1950; F3, fixed W using non-varying W of the year 1950; F4, fixed POP using non-varying POP values of the year 1950; F5, fixed RUR using non-varying RUR values of the year 1950; and F6, fixed DIS using non-varying DIS values of the year 1950. F0 was "all varying," with all varying factors considered (i.e., the offline historical simulation). The six formulas (F0–F1, F0–F2, F0–F3, F0–F4, F0–F5, and F0–F6) were used to evaluate the effects of T, P, W, POP, RUR, and DIS limiting factors on the BA trend. The limiting factors for a change in present-day BA trend were explored using offline simulations over the period 1987–2016.

Factorial analysis on the long-term BA-limiting factors

Similar to the factorial experiments F1–F6 in the last section, a second set of factorial analyses was performed to explore the roles of different limiting factors in the long-term global BA dynamics over the period 1860–2100 using a fully coupled framework in the S3 scenario (Table 1). Therefore, here, baseline CRU climatology was used to replace "the climate of the year 1950" in F1–F3 runs to represent constant climate. This was forced by three ESMs, IPSL-CM5A-MR, CSIRO-Mk3-6-0, and MIROC-ESM, which projected the maximum, minimum, and mid-range P, respectively, in the year 2100 (Note S4).

Human impacts on BA dynamics

Population growth and urbanization are the important factors in determining BA dynamics. However, our study was designed based on only the four experiment scenarios, i.e., specific combinations of future demographic scenarios with CO_2 emission scenarios were used (Table 1). To better understanding and clarify the priority in sequence of the human impacts on global BA dynamics, a sensitivity analysis under the intermediate CO_2 emission scenario (RCP6.0) was performed, exploring all combinations of population growth/urbanization rates within SSPs, i.e., nine combinations (3 population growth rate × 3 urbanization rate) with different levels (slow, middle, and rapid in Table 1) of population growth and urbanization rates. This coupled run was forced by one ESM: MIROC-ESM.

Drivers of future BA trends

Different from the definition of dominant limiting factors, dominant drivers of BA trends were defined as the independent driving factor that contributed the most to the increase (or decrease) in BA trends in each grid cell without any interactive effects among factors. We performed a third set of factorial analysis (including seven runs): M1, varying T only; M2, varying P only; M3, varying W only; M4, varying POP only; M5, varying RUR only; and M6, varying DIS only. M0 was the "control experiment" with socioeconomic factors constant to the values at the year 1950 and climatic factors constant to the baseline CRU climatology. The six formulas (M1–M0, M2–M0, M3–M0, M4–M0, M5–M0, and M6–M0) were used to evaluate the drivers of T, P, W, POP, RUR, and DIS to the BA trend. The fraction of global burned land grid cells (%) where a change in BA trend was attributed to different dominant drivers was obtained by summing the number of grid cells with the same dominant driver and dividing by the total number of global burned land grid cells. Burned land grid cells were defined as the land grid cells with simulated mean annual BA larger than zero. The future projected drivers of BA trend were based on GISS-E2-R-CC ESM simulation over the last 30 years of the 21st century.

SUPPLEMENTAL INFORMATION

Supplemental information can be found online at https://doi.org/10.1016/j.oneear.2021.03.002.

ACKNOWLEDGMENTS

The simulations were performed on the platform of the University of Exeter, UK. We thank Jiafu Mao, Shushi Peng, Jun Yang, Felix Leung, Eleanor Burke, and Xuecao Li, who gave valuable comments about this work. We would also like to thank the editor and three anonymous reviewers for their valuable comments, which have contributed to an improved paper. Finally, we thank the GFED, FireCCI, CMIP5 database, ILAMB, and other researchers who worked to provide the datasets for this study. This work was supported by the National Natural Science Foundation of China (31570475), Tsinghua University-Peter the Great St. Petersburg Polytechnic University Joint Scientific Research Fund (20193080033), and the National Key R&D Program of China (2017YFA0604404) (C.W. and S.V.) and China Scholarship Council (C.W.). L.M.M. and S.S. were partly supported by the Newton Fund through Met Office Climate Science for Service Partnership Brazil (CSSP Brazil) and Natural Environment Research Council (NERC) grants (NE/R001812/1 and NE/J010057/1). L.M.M. was also partly supported by the UK Natural Environment Research Council through The UK Earth System Modeling Project (UKESM, grant NE/N017951/1). C.H. acknowledged the National Capability grant awarded to the UK Centre for Ecology and Hydrology by the Natural Environment Research Council. C.W. and A.C.S. were partially supported by a grant from the National Science Foundation to A.C.S. (MSB 1802453).

AUTHOR CONTRIBUTIONS

S.S., C.W., C.H., and S.V. designed the research; C.W. performed the simulations and analysis; C.W. wrote the first draft; and C.W., S.S., L.M.M., C.H., S.V., and A.C.S. contributed to the interpretation of the results and writing of the paper.

DECLARATION OF INTERESTS

The authors declare no competing interests.

Received: May 12, 2020
Revised: February 23, 2021
Accepted: March 4, 2021
Published: April 1, 2021

REFERENCES

1. Bowman, D.M., Balch, J.K., Artaxo, P., Bond, W.J., Carlson, J.M., Cochrane, M.A., D'Antonio, C.M., Defries, R.S., Doyle, J.C., Harrison, S.P., et al. (2009). Fire in the earth system. Science *324*, 481–484.
2. Veraverbeke, S., Rogers, B.M., Goulden, M.L., Jandt, R.R., Miller, C.E., Wiggins, E.B., and Randerson, J.T. (2017). Lightning as a major driver of recent large fire years in North American boreal forests. Nat. Clim. Chang. *7*, 529–534.
3. van der Werf, G.R., Randerson, J.T., Giglio, L., van Leeuwen, T.T., Chen, Y., Rogers, B.M., Mu, M., van Marle, M.J.E., Morton, D.C., Collatz, G.J., et al. (2017). Global fire emissions estimates during 1997–2016. Earth Syst. Sci. Data *9*, 697–720.
4. Moritz, M.A., Batllori, E., Bradstock, R.A., Gill, A.M., Handmer, J., Hessburg, P.F., Leonard, J., McCaffrey, S., Odion, D.C., Schoennagel, T., et al. (2014). Learning to coexist with wildfire. Nature *515*, 58–66.
5. Andela, N., Morton, D.C., Giglio, L., Chen, Y., van der Werf, G.R., Kasibhatla, P.S., DeFries, R.S., Collatz, G.J., Hantson, S., Kloster, S.,

et al. (2017). A human-driven decline in global burned area. Science *356*, 1356–1362.

6. Moritz, M.A., Parisien, M.A., Batllori, E., Krawchuk, M.A., Van Dorn, J., Ganz, D.J., and Hayhoe, K. (2012). Climate change and disruptions to global fire activity. Ecosphere *3*, 1–22.
7. Kloster, S., and Lasslop, G. (2017). Historical and future fire occurrence (1850 to 2100) simulated in CMIP5 Earth System Models. Glob. Planet. Change *150*, 58–69.
8. Pechony, O., and Shindell, D.T. (2010). Driving forces of global wildfires over the past millennium and the forthcoming century. Proc. Natl. Acad. Sci. U S A *107*, 19167–19170.
9. Krawchuk, M.A., Moritz, M.A., Parisien, M.A., Van Dorn, J., and Hayhoe, K. (2009). Global pyrogeography: the current and future distribution of wildfire. PLoS One *4*, e5102.
10. Knorr, W., Arneth, A., and Jiang, L. (2016). Demographic controls of future global fire risk. Nat. Clim. Chang. *6*, 781–785.
11. Bond, W.J., and Keeley, J.E. (2005). Fire as a global 'herbivore': the ecology and evolution of flammable ecosystems. Trends Ecol. Evol. *20*, 387–394.
12. Archibald, S., Roy, D.P., van Wilgen, B.W., and Scholes, R.J. (2009). What limits fire? An examination of drivers of burnt area in Southern Africa. Glob. Chang. Biol. *15*, 613–630.
13. Lasslop, G., and Kloster, S. (2017). Human impact on wildfires varies between regions and with vegetation productivity. Environ. Res. Lett. *12*, 115011.
14. Williams, A.P., Abatzoglou, J.T., Gershunov, A., Guzman-Morales, J., Bishop, D.A., Balch, J.K., and Lettenmaier, D.P. (2019). Observed impacts of anthropogenic climate change on wildfire in California. Earth's Future *7*, 892–910.
15. Thomas, P.B., Watson, P.J., Bradstock, R.A., Penman, T.D., and Price, O.F. (2014). Modelling surface fine fuel dynamics across climate gradients in eucalypt forests of south-eastern Australia. Ecography *37*, 827–837.
16. Lasslop, G., Hantson, S., and Kloster, S. (2015). Influence of wind speed on the global variability of burned fraction: a global fire model's perspective. Int. J. Wildland Fire *24*, 989–1000.
17. Flannigan, M.D., Logan, K.A., Amiro, B.D., Skinner, W.R., and Stocks, B.J. (2005). Future area burned in Canada. Clim. Change *72*, 1–16.
18. Marlon, J.R., Bartlein, P.J., Carcaillet, C., Gavin, D.G., Harrison, S.P., Higuera, P.E., Joos, F., Power, M.J., and Prentice, I.C. (2008). Climate and human influences on global biomass burning over the past two millennia. Nat. Geosci. *1*, 697–702.
19. Aragão, L.E.O.C., Malhi, Y., Barbier, N., Lima, A., Shimabukuro, Y., Anderson, L., and Saatchi, S. (2008). Interactions between rainfall, deforestation and fires during recent years in the Brazilian Amazonia. Philos. Trans. R. Soc. Lond. B Biol. Sci. *363*, 1779–1785.
20. Venevsky, S., Thonicke, K., Sitch, S., and Cramer, W. (2002). Simulating fire regimes in human-dominated ecosystems: Iberian Peninsula case study. Glob. Chang. Biol. *8*, 984–998.
21. Bistinas, I., Harrison, S.P., Prentice, I.C., and Pereira, J.M.C. (2014). Causal relationships versus emergent patterns in the global controls of fire frequency. Biogeosciences *11*, 5087–5101.
22. Keeley, J.E., and Syphard, A.D. (2018). Historical patterns of wildfire ignition sources in California ecosystems. Int. J. Wildland Fire *27*, 781–799.
23. Radeloff, V.C., Helmers, D.P., Kramer, H.A., Mockrin, M.H., Alexandre, P.M., Bar-Massada, A., Butsic, V., Hawbaker, T.J., Martinuzzi, S., Syphard, A.D., et al. (2018). Rapid growth of the US wildland-urban interface raises wildfire risk. Proc. Natl. Acad. Sci. U S A *115*, 3314–3319.
24. McDonald, R.I., Forman, R.T.T., Kareiva, P., Neugarten, R., Salzer, D., and Fisher, J. (2009). Urban effects, distance, and protected areas in an urbanizing world. Landscape Urban Plann. *93*, 63–75.
25. Price, O., and Bradstock, R. (2014). Countervailing effects of urbanization and vegetation extent on fire frequency on the Wildland Urban Interface: Disentangling fuel and ignition effects. Landscape Urban Plann. *130*, 81–88.
26. Venevsky, S., Le Page, Y., Pereira, J.M.C., and Wu, C. (2019). Analysis fire patterns and drivers with a global SEVER-FIRE v1.0 model incorporated into dynamic global vegetation model and satellite and on-ground observations. Geosci. Model Dev. *12*, 89–110.
27. Schoennagel, T., Nelson, C.R., Theobald, D.M., Carnwath, G.C., and Chapman, T.B. (2009). Implementation of National Fire Plan treatments near the wildland-urban interface in the western United States. Proc. Natl. Acad. Sci. U S A *106*, 10706–10711.
28. Syphard, A.D., Radeloff, V.C., Keeley, J.E., Hawbaker, T.J., Clayton, M.K., Stewart, S.I., and Hammer, R.B. (2007). Human influence on California fire regimes. Ecol. Appl. *17*, 1388–1402.
29. Bowman, D.M.J.S., Balch, J., Artaxo, P., Bond, W.J., Cochrane, M.A., D'Antonio, C.M., DeFries, R., Johnston, F.H., Keeley, J.E., Krawchuk, M.A., et al. (2011). The human dimension of fire regimes on Earth. J. Biogeogr. *38*, 2223–2236.
30. Ingalsbee, T., and Raja, U. (2015). Chapter 12 - the rising costs of wildfire suppression and the case for ecological fire use. In The Ecological Importance of Mixed-Severity Fires, D.A. DellaSala and C.T. Hanson, eds. (Elsevier), pp. 348–371.
31. Walters, G. (2012). Customary fire regimes and vegetation structure in Gabon's Bateke Plateaux. Hum. Ecol. *40*, 943–955.
32. Maezumi, S.Y., Robinson, M., de Souza, J., Urrego, D.H., Schaan, D., Alves, D., and Iriarte, J. (2018). New insights from pre-columbian land use and fire management in Amazonian Dark earth forests. Front. Ecol. Evol. *6*, 111.
33. Walters, G. (2015). Changing fire governance in Gabon's Plateaux Bateke savanna landscape. Conserv. Soc. *13*, 275–286.
34. Fonseca-Morello, T., Ramos, R., Steil, L., Parry, L., Barlow, J.O.S., Markusson, N., and Ferreira, A. (2017). Fires in Brazilian amazon: why does policy have a limited impact? Ambient. Soc. *20*, 19–38.
35. Wu, C., Venevsky, S., Sitch, S., Yang, Y., Wang, M.H., Wang, L., and Gao, Y. (2017). Present-day and future contribution of climate and fires to vegetation composition in the boreal forest of China. Ecosphere *8*, e01917.
36. Sitch, S., Smith, B., Prentice, I.C., Arneth, A., Bondeau, A., Cramer, W., Kaplan, J.O., Levis, S., Lucht, W., Sykes, M.T., et al. (2003). Evaluation of ecosystem dynamics, plant geography and terrestrial carbon cycling in the LPJ dynamic global vegetation model. Glob. Chang. Biol. *9*, 161–185.
37. Sitch, S., Huntingford, C., Gedney, N., Levy, P.E., Lomas, M., Piao, S.L., Betts, R., Ciais, P., Cox, P., Friedlingstein, P., et al. (2008). Evaluation of the terrestrial carbon cycle, future plant geography and climate-carbon cycle feedbacks using five Dynamic Global Vegetation Models (DGVMs). Glob. Chang. Biol. *14*, 2015–2039.
38. Sitch, S., Friedlingstein, P., Gruber, N., Jones, S.D., Murray-Tortarolo, G., Ahlstrom, A., Doney, S.C., Graven, H., Heinze, C., Huntingford, C., et al. (2015). Recent trends and drivers of regional sources and sinks of carbon dioxide. Biogeosciences *12*, 653–679.
39. Gerten, D., Schaphoff, S., Haberlandt, U., Lucht, W., and Sitch, S. (2004). Terrestrial vegetation and water balance—hydrological evaluation of a dynamic global vegetation model. J. Hydrol. *286*, 249–270.
40. Huntingford, C., Booth, B.B.B., Sitch, S., Gedney, N., Lowe, J.A., Liddicoat, S.K., Mercado, L.M., Best, M.J., Weedon, G.P., Fisher, R.A., et al. (2010). IMOGEN: an intermediate complexity model to evaluate terrestrial impacts of a changing climate. Geosci. Model. Dev. *3*, 679–687.
41. Harris, I., Jones, P.D., Osborn, T.J., and Lister, D.H. (2013). Updated high--resolution grids of monthly climatic observations – the CRU TS3.10 Dataset. Int. J. Climatol. *34*, 623–642.
42. Moss, R.H., Edmonds, J.A., Hibbard, K.A., Manning, M.R., Rose, S.K., van Vuuren, D.P., Carter, T.R., Emori, S., Kainuma, M., Kram, T., et al. (2010). The next generation of scenarios for climate change research and assessment. Nature *463*, 747–756.
43. Riahi, K., van Vuuren, D.P., Kriegler, E., Edmonds, J., O'Neill, B.C., Fujimori, S., Bauer, N., Calvin, K., Dellink, R., Fricko, O., et al. (2017). The Shared Socioeconomic Pathways and their energy, land use, and

greenhouse gas emissions implications: an overview. Glob. Environ. Change *42*, 153–168.

44. Zhang, T., Wooster, M., de Jong, M., and Xu, W. (2018). How well does the 'small fire boost' methodology used within the GFED4.1s fire emissions database represent the timing, location and magnitude of agricultural burning? Remote Sen. *10*, 823.
45. Chuvieco, E., Lizundia-Loiola, J., Pettinari, M.L., Ramo, R., Padilla, M., Tansey, K., Mouillot, F., Laurent, P., Storm, T., Heil, A., et al. (2018). Generation and analysis of a new global burned area product based on MODIS 250 m reflectance bands and thermal anomalies. Earth Syst. Sci. Data *10*, 2015–2031.
46. Collier, N., Hoffman, F.M., Lawrence, D.M., Keppel-Aleks, G., Koven, C.D., Riley, W.J., Mu, M., and Randerson, J.T. (2018). The international land model benchmarking (ILAMB) system: Design, theory, and implementation. J. Adv. Model. Earth Syst. *10*, 2731–2754.
47. Poulter, B., MacBean, N., Hartley, A., Khlystova, I., Arino, O., Betts, R., Bontemps, S., Boettcher, M., Brockmann, C., Defourny, P., et al. (2015). Plant functional type classification for earth system models: results from the European Space Agency's Land Cover Climate Change Initiative. Geosci. Model. Dev. *8*, 2315–2328.
48. Kelley, D.I., Bistinas, I., Whitley, R., Burton, C., Marthews, T.R., and Dong, N. (2019). How contemporary bioclimatic and human controls change global fire regimes. Nat. Clim. Chang. *9*, 690–696.
49. Zhu, Z.C., Piao, S.L., Myneni, R.B., Huang, M.T., Zeng, Z.Z., Canadell, J.G., Ciais, P., Sitch, S., Friedlingstein, P., Arneth, A., et al. (2016). Greening of the earth and its drivers. Nat. Clim. Chang. *6*, 791–795.
50. Kc, S., and Lutz, W. (2017). The human core of the shared socioeconomic pathways: population scenarios by age, sex and level of education for all countries to 2100. Glob. Environ. Change *42*, 181–192.
51. Jung, M., Reichstein, M., Schwalm, C.R., Huntingford, C., Sitch, S., Ahlstrom, A., Arneth, A., Camps-Valls, G., Ciais, P., Friedlingstein, P., et al. (2017). Compensatory water effects link yearly global land CO2 sink changes to temperature. Nature *541*, 516–520.
52. Ludewigs, T., D'antona, A.d.O., Brondízio, E.S., and Hetrick, S. (2009). Agrarian structure and land-cover change along the lifespan of three colonization areas in the Brazilian amazon. World Dev. *37*, 1348–1359.
53. Steel, G., Birch-Thomsen, T., Cottyn, I., Lazaro, E.A., Mainet, H., Mishili, F.J., and van Lindert, P. (2019). Multi-activity, multi-locality and small-town development in Cameroon, Ghana, Rwanda and Tanzania. Eur. J. Dev. Res. *31*, 12–33.
54. Chas-Amil, M.L., Prestemon, J.P., McClean, C.J., and Touza, J. (2015). Human-ignited wildfire patterns and responses to policy shifts. Appl. Geogr. *56*, 164–176.
55. de Groot, W.J., Flannigan, M.D., and Cantin, A.S. (2013). Climate change impacts on future boreal fire regimes. For. Ecol. Manage. *294*, 35–44.
56. Kasischke, E.S., and Turetsky, M.R. (2006). Recent changes in the fire regime across the North American boreal region—spatial and temporal patterns of burning across Canada and Alaska. Geophys. Res. Lett. *33*, L0970.
57. Eby, M., Zickfeld, K., Montenegro, A., Archer, D., Meissner, K.J., and Weaver, A.J. (2009). Lifetime of anthropogenic climate change: Millennial time scales of potential CO2 and surface temperature perturbations. J. Clim. *22*, 2501–2511.
58. Smith, T.M., and Shugart, H.H. (1993). The transient response of terrestrial carbon storage to a perturbed climate. Nature *361*, 523–526.
59. Aragao, L., Anderson, L.O., Fonseca, M.G., Rosan, T.M., Vedovato, L.B., Wagner, F.H., Silva, C.V.J., Silva Junior, C.H.L., Arai, E., Aguiar, A.P., et al. (2018). 21st Century drought-related fires counteract the decline of Amazon deforestation carbon emissions. Nat. Commun. *9*, 536.
60. Aragão, L.E.O.C., and Shimabukuro, Y.E. (2010). The incidence of fire in Amazonian forests with implications for REDD. Science *328*, 1275–1278.
61. Barlow, J., Parry, L., Gardner, T.A., Ferreira, J., Aragão, L.E.O.C., Carmenta, R., Berenguer, E., Vieira, I.C.G., Souza, C., and Cochrane, M.A. (2012). The critical importance of considering fire in REDD+ programs. Biol. Conserv. *154*, 1–8.
62. Ruffault, J., and Mouillot, F. (2015). How a new fire-suppression policy can abruptly reshape the fire-weather relationship. Ecosphere *6*, art199.
63. Fréjaville, T., and Curt, T. (2017). Seasonal changes in the human alteration of fire regimes beyond the climate forcing. Environ. Res. Lett. *12*, 035006.
64. Ruffault, J., Curt, T., Moron, V., Trigo, R.M., Mouillot, F., Koutsias, N., Pimont, F., Martin-StPaul, N., Barbero, R., Dupuy, J.-L., et al. (2020). Increased likelihood of heat-induced large wildfires in the Mediterranean Basin. Sci. Rep. *10*, 13790.
65. Riley, K.L., Thompson, M.P., Scott, J.H., and Gilbertson-Day, J.W. (2018). A model-based framework to evaluate alternative wildfire suppression strategies. Resources *7*, 4.
66. Brotons, L., Aquilué, N., de Cáceres, M., Fortin, M.-J., and Fall, A. (2013). How fire history, fire suppression practices and climate change affect wildfire regimes in Mediterranean landscapes. PLoS One *8*, e62392.
67. Scholze, M., Knorr, W., Arnell, N.W., and Prentice, I.C. (2006). A climate-change risk analysis for world ecosystems. Proc. Natl. Acad. Sci. U S A *103*, 13116–13120.
68. Le Page, Y., Morton, D., Bond-Lamberty, B., Pereira, J.M.C., and Hurtt, G. (2015). HESFIRE: a global fire model to explore the role of anthropogenic and weather drivers. Biogeosciences *12*, 887–903.
69. Fischer, A.P., Spies, T.A., Steelman, T.A., Moseley, C., Johnson, B.R., Bailey, J.D., Ager, A.A., Bourgeron, P., Charnley, S., Collins, B.M., et al. (2016). Wildfire risk as a socioecological pathology. Front. Ecol. Environ. *14*, 276–284.
70. Korontzi, S., McCarty, J., Loboda, T., Kumar, S., and Justice, C. (2006). Global distribution of agricultural fires in croplands from 3 years of Moderate Resolution Imaging Spectroradiometer (MODIS) data. Glob. Biogeochem. Cycles *20*, GB2021.
71. Andela, N., and van der Werf, G.R. (2014). Recent trends in African fires driven by cropland expansion and El Nino to La Nina transition. Nat. Clim. Chang. *4*, 791–795.
72. Pereira, J.M.C., Oom, D., Pereira, P., Turkman, A.A., and Turkman, K.F. (2015). Religious affiliation modulates weekly cycles of cropland burning in sub-saharan Africa. PLoS One *10*, e0139189.
73. Kelley, D.I., and Harrison, S.P. (2014). Enhanced Australian carbon sink despite increased wildfire during the 21st century. Environ. Res. Lett. *9*, 104015.
74. Hantson, S., Arneth, A., Harrison, S.P., Kelley, D.I., Prentice, I.C., Rabin, S.S., Archibald, S., Mouillot, F., Arnold, S.R., Artaxo, P., et al. (2016). The status and challenge of global fire modelling. Biogeosciences *13*, 3359–3375.
75. Huntingford, C., and Cox, P.M. (2000). An analogue model to derive additional climate change scenarios from existing GCM simulations. Clim. Dyn. *16*, 575–586.
76. Huntingford, C., Zelazowski, P., Galbraith, D., Mercado, L.M., Sitch, S., Fisher, R., Lomas, M., Walker, A.P., Jones, C.D., Booth, B.B.B., et al. (2013). Simulated resilience of tropical rainforests to CO2-induced climate change. Nat. Geosci. *6*, 268–273.
77. Huntingford, C., Atkin, O.K., Martinez-de la Torre, A., Mercado, L.M., Heskel, M.A., Harper, A.B., Bloomfield, K.J., O'Sullivan, O.S., Reich, P.B., Wythers, K.R., et al. (2017). Implications of improved representations of plant respiration in a changing climate. Nat. Commun. *8*, 1602.
78. Kalnay, E., Kanamitsu, M., Kistler, R., Collins, W., Deaven, D., Gandin, L., Iredell, M., Saha, S., White, G., Woollen, J., et al. (1996). The NCEP/NCAR 40-year reanalysis project. Bull. Am. Meteorol. Soc. *77*, 437–472.
79. Meinshausen, M., Smith, S.J., Calvin, K., Daniel, J.S., Kainuma, M.L.T., Lamarque, J.F., Matsumoto, K., Montzka, S.A., Raper, S.C.B., Riahi, K., et al. (2011). The RCP greenhouse gas concentrations and their extensions from 1765 to 2300. Clim. Change *109*, 213–241.
80. New, M., Hulme, M., and Jones, P. (2000). Representing twentieth-century space-time climate variability. Part II: development of 1901-96 monthly grids of terrestrial surface climate. J. Clim. *13*, 2217–2238.

81. Seto, K.C., Guneralp, B., and Hutyra, L.R. (2012). Global forecasts of urban expansion to 2030 and direct impacts on biodiversity and carbon pools. Proc. Natl. Acad. Sci. U S A *109*, 16083–16088.

82. Bettencourt, L.M., Lobo, J., Helbing, D., Kuhnert, C., and West, G.B. (2007). Growth, innovation, scaling, and the pace of life in cities. Proc. Natl. Acad. Sci. U S A *104*, 7301–7306.

83. Angel, S., Parent, J., Civco, D.L., Blei, A., and Potere, D. (2011). The dimensions of global urban expansion: estimates and projections for all countries, 2000-2050. Prog. Plann. *75*, 53–107.

84. Liu, Y., and Phinn, S.R. (2003). Modelling urban development with cellular automata incorporating fuzzy-set approaches. Comput. Environ. Urban Syst. *27*, 637–658.

85. Millward, H. (2005). Rural population change in Nova Scotia, 1991–2001: bivariate and multivariate analysis of key drivers. Can. Geogr. *49*, 180–197.

86. Lasslop, G., Hantson, S., Harrison, S.P., Bachelet, D., Burton, C., Forkel, M., Forrest, M., Li, F., Melton, J.R., Yue, C., et al. (2020). Global ecosystems and fire: Multi-model assessment of fire-induced tree-cover and carbon storage reduction. Glob. Chang. Biol. *26*, 5027–5041.

87. Bond, W.J., Woodward, F.I., and Midgley, G.F. (2005). The global distribution of ecosystems in a world without fire. New Phytol. *165*, 525–537.

88. Giglio, L., Randerson, J.T., van der Werf, G.R., Randerson, J.T., Chen, Y., van der Werf, G.R., Rogers, B.M., and Morton, D.C. (2013). Analysis of daily, monthly, and annual burned area using the fourth-generation global fire emissions database (GFED4). J. Geophys. Res. Biogeosci. *118*, 317–328.